Temporal Interpolation Methods for the Clouds and the Earth's Radiant Energy System (CERES) Experiment

D. F. YOUNG AND P. MINNIS

Atmospheric Sciences Division, NASA/Langley Research Center, Hampton, Virginia

D. R. DOELLING

Analytical Services & Materials, Inc., Hampton, Virginia

G. G. GIBSON AND T. WONG

Atmospheric Sciences Division, NASA/Langley Research Center, Hampton, Virginia

(Manuscript received 31 May 1997, in final form 31 October 1997)

ABSTRACT

The Clouds and the Earth's Radiant Energy System (CERES) is a NASA multisatellite measurement program for monitoring the radiation environment of the earth–atmosphere system. The CERES instrument was flown on the Tropical Rainfall Measuring Mission satellite in late 1997, and will be flown on the Earth Observing System morning satellite in 1998 and afternoon satellite in 2000. To minimize temporal sampling errors associated with satellite measurements, two methods have been developed for temporally interpolating the CERES earth radiation budget measurements to compute averages of top-of-the-atmosphere shortwave and longwave flux. The first method is based on techniques developed from the Earth Radiation Budget Experiment (ERBE) and provides radiation data that are consistent with the ERBE processing. The second method is a newly developed technique for use in the CERES data processing. This technique incorporates high temporal resolution data from geostationary satellites to improve modeling of diurnal variations of radiation due to changing cloud conditions during the day. The performance of these two temporal interpolation methods is evaluated using a simulated dataset. Simulation studies show that the introduction of geostationary data into the temporal interpolation process significantly improves the accuracy of hourly and daily radiative products. Interpolation errors for instantaneous flux estimates are reduced by up to 68% for longwave flux and 80% for shortwave flux.

1. Introduction

Global radiation budget measurements at the top of the atmosphere (TOA) are fundamental quantities for monitoring the earth's climate system. These important climatic measurements have traditionally been obtained from earth radiation budget (ERB) instruments on board polar-orbiting satellites. While these satellites are capable of viewing the entire earth's surface from the North Pole to the South Pole over a number of satellite orbital passes, they do not, however, provide continuous spatial coverage of the earth's entire surface at any one specific time or continuous temporal coverage for any one specific location on the earth. The sparse distribution of these satellite measurements is the most critical factor affecting temporal averaging of radiation data from regional to global scales (Brooks et al. 1986). To overcome these sampling problems and to recapture the proper daily or monthly average of these radiation parameters, realistic temporal models of the diurnal variability of the earth's radiation fields are required. Specifically, these diurnal models must adequately account for the solar zenith dependence of albedo and longwave exitance, as well as dependence of the radiation field on surface type and cloud cover.

Early radiation budget satellite experiments in the mid-1970s used very simple procedures to obtain daily averages of longwave (LW) and reflected shortwave (SW) radiation. For example, National Oceanic and Atmospheric Administration (NOAA) scanning radiometer data (Gruber and Winston 1978) and *Nimbus-6* ERB experiment (Jacobowitz et al. 1979) data assumed that daily albedo in a region equals the albedo at the local time of the measurement and ignored the substantial diurnal variation of albedo with solar zenith angle and changes of cloudiness during the day. Similarly, daily LW flux was computed as the unweighted mean of daytime and nighttime measurements and neglected the importance of the diurnal cycle of LW flux, which is es-

Corresponding author address: Mr. David F. Young, NASA/Langley Research Center, Mail Stop 420, Hampton, VA 23681.
E-mail: d.f.young@larc.nasa.gov

pecially pronounced over land and desert regions. These temporal modeling problems were reduced by incorporating empirical surface-dependent albedo models developed from *Nimbus-2* and *-3* satellite data to account for solar-zenith-angle dependence of reflected SW flux and length-of-day weighting factors in averaging the daytime and nighttime LW flux (Raschke et al. 1973; Raschke and Bandeen 1970). Further developments and improvements of the surface-dependent angular reflectance models continued in the early 1980s using *Nimbus-7* radiance data (Taylor and Stowe 1984). These improved models were applied to the *Nimbus-7* measurements to obtain radiation budget data with corrections to daily albedo based on models from *Nimbus-3.*

The launch of the Earth Radiation Budget Experiment (ERBE; Barkstrom 1984; Barkstrom and Smith 1986) in the mid-1980s opened a new chapter in earth radiation budget measurements. ERBE incorporated many technological advances in instrumentation, as well as improved techniques for diurnal averaging. For example, 12 new directional models based on *Nimbus-7* and Geostationary Operational Environmental Satellite (GOES) measurements (Suttles et al. 1988) were used to refine diurnal interpolation of albedo. A new half-sine model based on GOES observations (Brooks and Minnis 1984a) was used to improve the diurnal interpolation of LW flux over desert and vegetated land surfaces. In addition, ERBE made the first attempt to account for diurnal variations in clouds by measuring the radiation budget with multiple satellites (Harrison et al. 1983). This multisatellite system included the precessing Earth Radiation Budget Satellite (ERBS), which sampled latitudes between 60°S and 60°N and covered all local times at the equator in 36 days, and the *NOAA-9* and *-10* sun-synchronous satellites with nominal ascending node equatorial crossing times of 1430 and 1930 local standard time (LST), respectively. This combination of multiple satellites and new diurnal models has produced the most accurate monthly mean regional albedos and LW fluxes to date (Harrison et al. 1988; Harrison et al. 1990; Barkstrom et al. 1990), as well as the best estimates of the diurnal variability of TOA radiative fluxes (Harrison et al. 1988; Hartmann et al. 1991).

The ERBS and *NOAA-9* scanning radiometers operated together for 2 years from February 1985 through January 1987, while ERBS and *NOAA-10* scanned simultaneously from December 1986 through May 1989. The highest accuracy was achieved during the 1 month when all three satellites had operating scanners. The two-satellite combinations represent a significant improvement over a single satellite (e.g., Brooks and Minnis 1984b). In some regions, however, errors in the monthly mean diurnal cycle of LW and SW fluxes can still be significant due to deviations from the assumed models.

The Clouds and the Earth's Radiant Energy System (CERES; Wielicki et al. 1996) is planned for flight on multiple satellite platforms starting in 1997 with the Tropical Rainfall Measuring Mission (TRMM) and on the Earth Observing System Morning Satellite and Afternoon Satellite (EOS-AM and EOS-PM) missions in 1998 and 2000, respectively. CERES represents a continuation of the ERBE dataset as well as an evolution in ERB technology to obtain more accurate satellite measurements and to develop and apply improved diurnal models. The temporal coverage of the three CERES satellites (TRMM, EOS-AM, and EOS-PM) for 1 month of observations is shown in Fig. 1. The TRMM spacecraft is in a 35° inclined, precessing orbit that covers all local times at the equator in slightly over 23 days. The EOS satellites are in sun-synchronous orbits, sampling at the same local times each day. From Fig. 1, it is evident that a single satellite cannot provide sufficient temporal sampling to accurately estimate SW and LW fluxes at all local hours. As with ERBE, the application of diurnal models will be required to obtain accurate monthly averages of radiation parameters. Also, the goals of CERES are more ambitious in that accurate hourly flux estimates are desired in addition to the monthly averages obtained by ERBE.

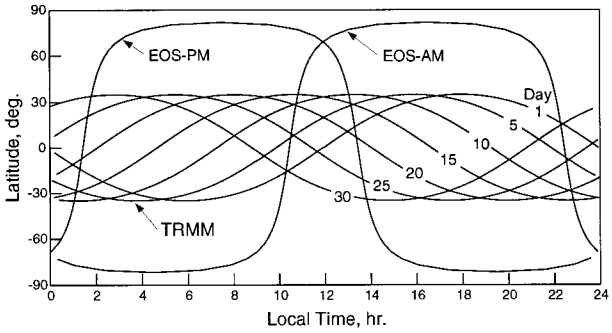

FIG. 1. Temporal coverage of CERES satellites.

As ERB satellite instrumentation has steadily improved over the years, models and methods for averaging and interpreting the data have undergone a similar evolutionary trend. From simple linear averaging to the more physically realistic ERBE models, the science of diurnal modeling attempts to expand the limited number of measurements into a complete time series of ERB information. The ERBE data analysis philosophy dictated the application of time–space averaging (TSA) methods that do not require any auxiliary data. While this approach proved quite successful in obtaining monthly average radiative parameters, individual days and hours were not accurately estimated. For future ERB missions such as CERES, a new TSA method will be explored involving the use of auxiliary geostationary satellite data to account for changing meteorological conditions during the day. Geostationary satellites can obtain a very high temporal sampling of their field of view, but data are typically available only every 3 h on a global basis (e.g., the International Satellite Cloud Climatology Project dataset).

This paper describes and evaluates the new temporal interpolation methods for CERES, the next generation of ERB satellite missions. CERES will produce monthly mean TOA fluxes using two methods. The first product will be produced in a manner identical with that used by ERBE. Since the ERBE TSA technique has evolved significantly since it was first described by Brooks et al. (1986), the first section of this paper documents its evolution. The subsequent section details a methodology for using geostationary data in the diurnal averaging process during the CERES mission. The expected improvement in accuracy of the geostationary-data-enhanced method relative to the ERBE methodology is also described.

2. Method I: ERBE-like time–space averaging

The chief input to CERES time–space averaging is a stream of satellite observations of SW and LW TOA flux. Included with each pixel measurement are the satellite viewing geometry, the latitude and longitude of the observation, the underlying geographic scene type, and the cloud category for the observed area. Additional input data include the solar declination angle and directional albedo models based on the angular distribution models (ADMs) of Suttles et al. (1988). The TSA process produces means of TOA SW and LW fluxes on various timescales ranging from hourly to monthly and on regional, zonal, and global spatial scales. Separate averages are computed for clear-sky and total-sky fluxes.

The ERBE methodology for temporally interpolating LW and SW radiation to all hours of the day for both clear-sky and total-sky conditions is outlined below.

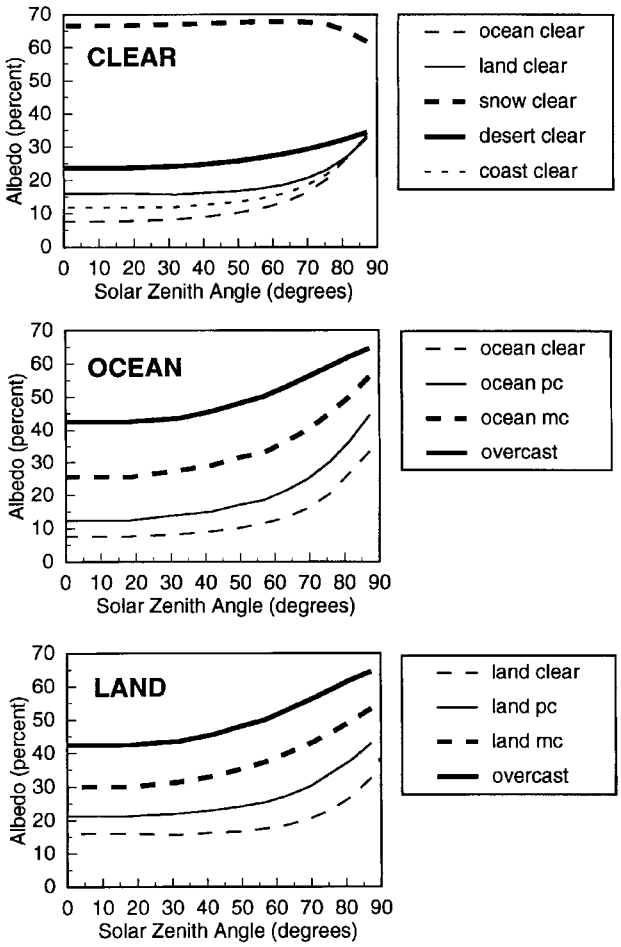

FIG. 2. ERBE models with variation of albedo as a function of solar zenith angle.

a. Spatial averaging and temporal corrections

The first step in the averaging process is to sort the chronologically ordered stream of flux measurements in space and time. Spatially, these data are averaged and processed on a geographical grid (e.g., 2.5° × 2.5° for ERBE). Each region (grid box) is processed independently from all others. Within each region, a month of ERB measurements is sorted and averaged into local time intervals of 1 h (referred to as hour boxes). There is a maximum of 744 hour boxes in a month (24 h per day times 31 days).

The averaging of the LW flux is straightforward. All observations from a region that were measured within an hour box are linearly combined. Since albedo is a function of solar zenith angle, each SW measurement is first corrected to the central time, latitude, and longitude of the regional hour box into which it is collected. The temporal correction is performed using the set of ADMs. As shown in Fig. 2, there are separate ADMs for the different clear-sky geographical scene types (ocean, land, snow, desert, and coast). The four ERBE cloud cover classes are clear (less than 5%), partly cloudy (5%–50%), mostly cloudy (50%–95%), and overcast (greater than 95%). Over land and ocean surfaces, there are models for partly cloudy and mostly cloudy ERBE scene classifications. The various cloud models over land are also used over desert and snow regions. A single model is used for overcast conditions over all surfaces. The ADMs for partly and mostly cloudy coastal scenes are not shown. Within each hour box, a separate mean albedo is calculated for each cloud class. The geographic scene type for each region is constant for a month.

b. Total-sky TOA LW flux

The ERBE TSA algorithm was designed to provide daily model fits to the TOA LW flux data, as well as monthly averages of these data. To accomplish this goal, an estimate of LW flux is made for every hour box. This interpolation is performed in one of two ways, depending on the geographic scene type of the region.

Over ocean regions, there is little diurnal variability in LW flux due to solar insolation. The greatest varia-

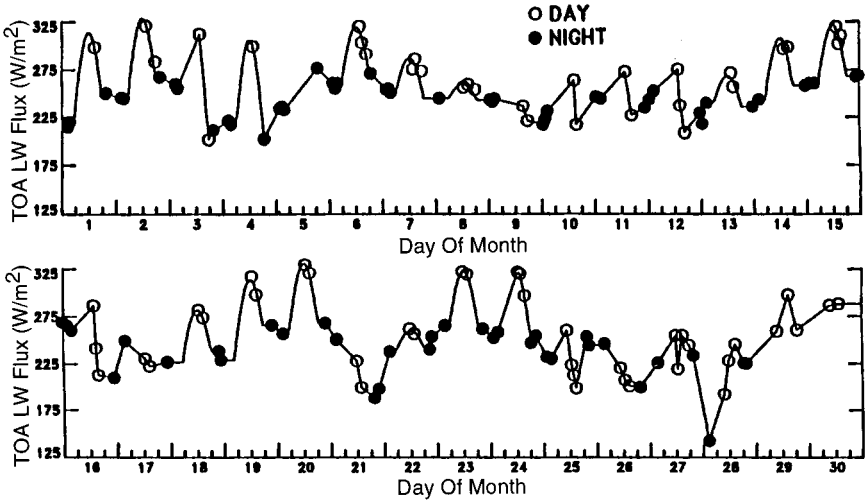

FIG. 3. Time series of ERBS and *NOAA-9* ERBE scanner TOA LW flux data and diurnal models for a 2.5° region in eastern New Mexico in April 1985.

tions in LW flux over the oceans occur due to changes in the amount and types of clouds. Therefore, no attempt is made to develop complex models for estimating the LW flux between the times of observations. Rather, it is assumed that changes in LW flux are due to changes in cloud conditions, and that such changes are linear. Thus, linear interpolation is used to provide a value of LW flux for each hour box not observed by the satellite. At the beginning of the month, all hours preceding the first observation are filled with the value from the first observed time. Similarly, the final measurement at the end of the month serves as the value for all remaining hours in the month. This technique is also used for regions designated as either snow-covered or coastal.

Over land and desert regions, the effects of solar heating are much more pronounced than over ocean regions. During relatively cloud-free periods, there is a generally sinusoidal variation in LW flux over the daylight hours (e.g., Minnis and Harrison 1984). To account for this variation, the LW flux for land and desert regions is interpolated in the following manner. For any day in which an observation was made during daylight hours, and during the preceding and following nights, the LW flux for the remaining daylight hours is modeled by fitting a half-sine curve to the observations. Linear interpolation substitutes for the half-sine modeling on days lacking the required observations, or when any daylight observations of LW flux are less than the adjacent nighttime values, or when the resultant half-sine curve has a negative amplitude.

Longwave interpolation is demonstrated in Fig. 3 using a time series of ERBE scanner data from April 1985 over a 2.5° region in eastern New Mexico. In this figure, observations are represented by circles and the interpolated values are displayed as the solid line. The early part of the month was relatively clear, and half-sine fits were performed on days 1, 2, 4, 6, 7, and 8. During days 10, 11, and 12, no half-sine fit was used since low values of LW were observed in the late afternoon, indicating that clouds must have been developing. In such cases, the half-sine fit is not realistic and linear interpolation is used.

When all hour boxes for the month have been filled with a value of LW flux, daily, monthly–hourly, and monthly means are calculated using two slightly different techniques. In the first method (monthly–daily), a daily mean is computed by averaging the 24 hour box values for each day; the monthly mean TOA LW flux, $\overline{F}_{\mathrm{LW}}$, is then computed by averaging all of the daily means as follows:

$$\overline{F}_{\mathrm{LW}} = \sum_{d=1}^{D} \left(\sum_{h=1}^{24} F_{\mathrm{LW}}(d, h)/24 \right) \Bigg/ D, \qquad (1)$$

where $F_{\mathrm{LW}}(d, h)$ is the TOA LW flux for day d and local hour h, and D is the total number of days in the month. In the second method (monthly–hourly), hour box values are averaged at each local hour for all days having an observation. The resulting 24 monthly–hourly means are then averaged to produce a monthly mean,

$$\overline{F}_{\mathrm{LW}} = \sum_{h=1}^{24} \left(\sum_{d=1}^{D_{\mathrm{LW}}} F_{\mathrm{LW}}(d, h)/D_{\mathrm{LW}} \right) \Bigg/ 24, \qquad (2)$$

where D_{LW} is the total number of days in the month with at least one LW measurement. The two estimates of monthly mean LW flux will be equal unless there were days during the month when no observations were made.

c. Clear-sky TOA LW flux

The above algorithm works well for total-sky LW flux in regions that are well sampled over most local times.

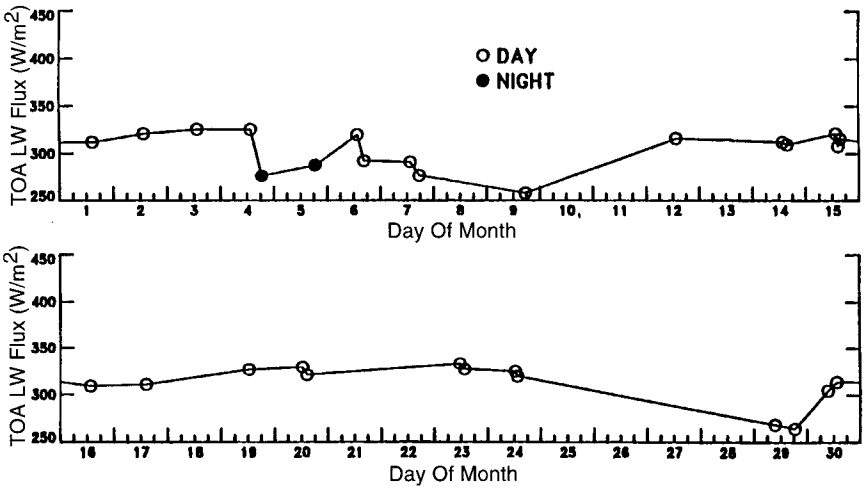

FIG. 4. Time series of ERBS and *NOAA*-9 ERBE scanner clear-sky TOA LW flux data and diurnal models for a 2.5° region in eastern New Mexico in April 1985.

However, problems may arise when applying this technique to clear-sky LW flux data. The ERBE cloud classification procedure is quite restrictive when classifying an observation as clear (Wielicki and Green 1989). Also, there are many regions over the globe where cloudy conditions prevail throughout the month. Consequently, a region may have a very limited number of clear-sky observations during the month. In addition, satellite sampling patterns may often cause a local time bias in the occurrence of clear-sky measurements. An example of this is shown in Fig. 4 for the same 2.5° ERBE region over New Mexico discussed above. For this case, with the exception of the two measurements from days 4 and 5, all of the limited number of clear-sky observations occurred during daylight hours. The lack of nighttime data means that the requirements for performing the diurnal half-sine fits are never met. Linear interpolation between the times of observation results in an unrealistically high monthly average because only daytime values are available. This problem is particularly serious over land and desert regions where large diurnal variations in clear-sky LW flux are expected. Since clear ocean areas have a much smaller LW flux diurnal variation, the day–night sampling bias should not severely affect the ocean monthly means. Therefore, in ocean regions, the clear-sky LW flux is averaged in a manner identical to the total-sky data.

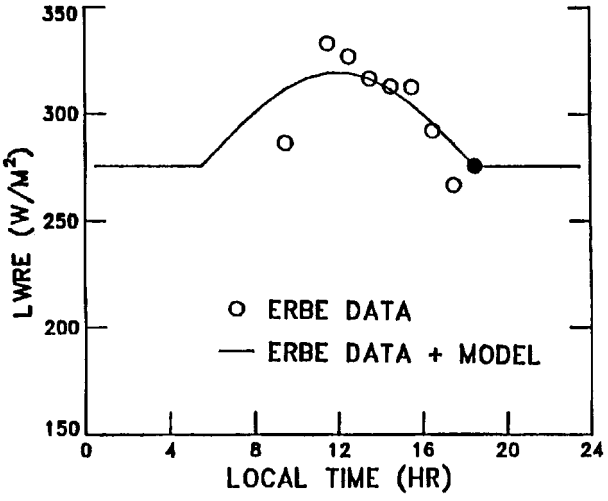

FIG. 5. ERBE time-averaged monthly–hourly clear-sky TOA LW flux results for the region shown in Fig. 4.

Because of the problems associated with obtaining accurate averages of clear-sky LW flux over land and deserts, the original ERBE TSA algorithm was modified to calculate only a single diurnal fit to the monthly ensemble of all clear-sky LW flux data. In the clear-sky case, it is reasonable to process all of the measurements together since the variance of measurements at the same local hour is expected to be small when compared with the total sky. There are, of course, some exceptions due to scene variability of the measurement footprints within the region, changing atmospheric conditions such as water vapor content and temperature during the month, cloud contamination of presumably clear-sky scenes, and possible error due to measurements being made at high viewing zenith angles. The underlying assumption is that this variability is small relative to the overall diurnal variation and can be effectively averaged out for a region having several clear-sky observations over the course of a month.

The clear-sky LW flux averaging technique is demonstrated in Fig. 5. The data shown in Fig. 4 have been sorted and averaged for the entire month in terms of local hour. The daytime points (open symbols) are then modeled using a least squares half-sine fit weighted by the number of measurements at each local hour during the month. The nighttime data (filled symbols) are simply averaged and the constant value is used for all night-

time hours. The monthly mean is then calculated by averaging the fit over 24 h if the fit meets five basic criteria.

1) There must be at least one daylight measurement located more than 1 h from the terminator.
2) There must be at least one nighttime measurement.
3) The least squares half-sine fit to the daylight data produces a positive amplitude.
4) The peak value of the fit must not exceed 400 W m^{-2}.
5) The length of day 15 of the month must be greater than 2 h.

If these criteria are not met, no monthly mean TOA LW clear-sky flux is calculated for the region. Since the modeling process is performed on data accumulated throughout the month, daily means are not calculated for land and desert regions.

This technique produces realistic values of monthly mean clear-sky LW flux, even in regions with sparse data sampling. However, there are many regions where no estimate can be made due to the total lack of nighttime, clear-sky data due to persistent overcast conditions or the overly restrictive ERBE clear classification scheme. To compensate for missing nighttime data, the clear-sky averaging algorithm attempts to correct for the misclassification of nighttime clear pixels as partly cloudy. For each nighttime hour box over land regions, a new clear-sky amount is estimated by assuming that 10% of the pixels classified as partly cloudy are actually clear when the region is classified as at least 50% partly cloudy. This is consistent with the mean ratio of clear to partly cloudy scene identification by ERBE in the daytime under these conditions. This new clear-sky amount can be used to calculate a value of clear-sky flux using the mean and standard deviation of the observed fluxes. If the maximum observed flux exceeds this value, then it is assumed to be clear and is used in the clear-sky averaging process. Although the global increase in clear-sky amount is slight (approximately 2%), the number of regions with no monthly mean clear-sky value is reduced by 60%–70%.

d. Total-sky and clear-sky TOA SW flux

The problem of producing diurnal, monthly–hourly, and monthly means of SW flux presents a different set of challenges from those associated with the LW flux. Because TOA SW flux is only pertinent to daylight hours, the problems involved in interpolating sparsely sampled LW data across day–night boundaries are not encountered. Furthermore, as shown in Fig. 2, there exist well-developed models of the variation of albedo with solar zenith angle for various clear and cloudy backgrounds (Suttles et al. 1988). These ADMs can be used to interpolate observations to other times of the day. The clear-sky SW flux (or albedo) can be modeled in the same manner as the total sky. The difficulties involved with the lack of nighttime clear-sky data are not a factor for SW interpolation.

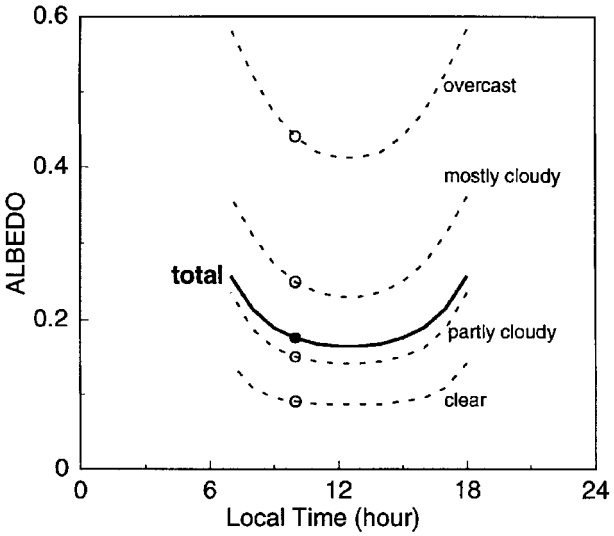

FIG. 6. Example of time interpolation of albedo for days with only 1 h of observation.

For each hour box with at least one observation, a mean albedo is calculated for each of the four ERBE cloud classifications: clear, partly cloudy, mostly cloudy, and overcast. A relative frequency histogram of each cloud classification is also stored. Because the temporal changes of SW radiation may be pronounced even within a single hour, measured values are first adjusted to the nearest local solar half-hour using the ADMs. For a given surface type and cloud cover category (i.e., scene type for selecting an ADM), the normalized ADM function, δ, is defined as the ratio of the ADM albedo at time t and the ADM albedo for overhead sun:

$$\delta_i[\mu_0(t)] = \alpha_{\mathrm{mod}_i}[\mu_0(t)]/\alpha_{\mathrm{mod}_i}(\mu_0 = 1), \qquad (3)$$

where μ_0 is the cosine of the solar zenith angle and α_{mod_i} is the ADM albedo for scene type i (from Fig. 2). The albedo at any time t' (e.g., at the local solar half-hour) can be expressed as the product of the observed albedo and the ratio of the normalized ADM functions from t' and the time of observation, t_{obs}:

$$\alpha_i(t') = \alpha_i[\mu_0(t_{\mathrm{obs}})]\delta_i[\mu_0(t')]/\delta_i[\mu_0(t_{\mathrm{obs}})]. \qquad (4)$$

For days with only one measurement of SW flux, each of the four cloud-type albedos from the hour of observation is modeled at all daylight hours using (4). This modeling is illustrated in Fig. 6. The albedos for the four cloud types are then recombined by weighting each cloud type albedo with the appropriate areal coverage fraction to obtain the mean albedo for each hour for the entire region (solid line in Fig. 6). The relative abundance of the cloud classifications is assumed to remain constant throughout the day.

For days with more than one measurement, this technique is modified as illustrated in Fig. 7. All daylight

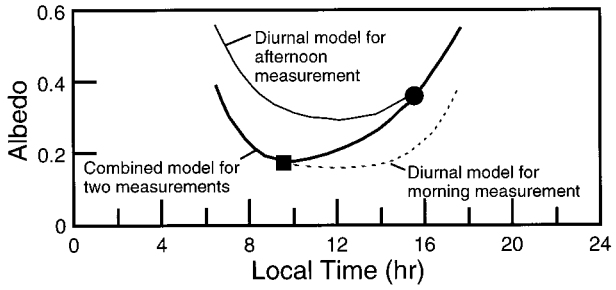

FIG. 7. Example of time interpolation of albedo with 2 h of observation during a day.

hours preceding the first measurement of the day and following the last measurement assume a constant cloud class from the nearest measurement. These hours are modeled using (4) as in the single measurement case. For hours between two measurements, it is assumed that the cloud histograms are varying linearly over that span. The four cloud-type albedos are modeled from each surrounding measurement using (4). Total albedo for each hour between the two measurements is then produced by inversely weighting the two estimates by the time from the hour of interest.

Monthly means are calculated when all hours are filled with albedo values for days with at least one measurement. Shortwave flux at each hour h of a given day d is

$$F_{\mathrm{SW}}(d, h) = E_0(d)\mu_0(d, h)\alpha(d, h), \tag{5}$$

where E_0 is the mean daily distance-corrected solar constant. The SW flux is summed over all hours of days with measurements and divided by a summation of solar incident flux over the same hours to produce a monthly mean albedo:

$$\overline{\alpha} = \sum_{d=1}^{D_{\mathrm{SW}}} \left(\sum_{h=1}^{24} F_{\mathrm{SW}}(d, h)/24 \right) \Bigg/ D_{\mathrm{SW}}/S_0, \tag{6}$$

where $F_{\mathrm{SW}}(d, h)$ is the TOA SW flux for day d and local hour h, D_{SW} is the total number of days in the month with at least one SW measurement, and S_0 is the summed solar incident SW flux. Monthly mean SW flux, $\overline{F}_{\mathrm{SW}}$, is then calculated by multiplying monthly mean albedo by the incident solar flux integrated and averaged over all hours of the month

$$\overline{F}_{\mathrm{SW}} = \overline{\alpha} S_0', \tag{7}$$

where S_0' is the integrated solar incident SW flux.

Means for the clear-sky SW flux are produced in a similar manner. In fact, the process is simpler than for the total-sky flux since only the clear albedo from each hour box needs to be interpolated to nonmeasured hours. Again, only days with at least one measurement are filled using the clear-sky ADMs, and values from these days are combined to produce daily, monthly–hourly, and monthly means.

e. Single versus multiple satellites

The ERBE TSA method was applied to datasets sampled from single and multiple CERES satellites to evaluate the accuracy of the estimated monthly means. The ''truth'' data field consists of hourly GOES data for July 1985; the analysis was limited to the area observed by GOES. The GOES reference (truth) data for LW and SW are given in Fig. 8. These flux data indicate generally clear conditions in the tropical eastern Pacific Ocean; high, thick clouds extending westward from South America just north of the equator; low stratocumulus clouds off the western U.S. coast; and a variety of cloud conditions over Northern Hemisphere land regions. A 1-month set of typical sampling times for crosstrack ERB instruments on the TRMM, EOS-AM, and EOS-PM satellites was computed using an orbital simulation computer program. The hourly GOES data were then subsampled at the satellite observation times and the ERBE TSA was applied as described in the previous sections. The error in the monthly average is then computed as the difference between the satellite-sampled monthly mean and the reference monthly mean from GOES.

The single satellite bias errors for TRMM, EOS-AM, and EOS-PM are shown in Figs. 9 and 10 for LW and SW, respectively. A TRMM initial equatorial crossing time of noon (1200) was used for this example, but crossing times of 0000, 0600, and 1800 LST were also simulated to cover the range of sampling that can occur with the precessing satellite. The TRMM satellite precesses through all local hours at the equator in about 23 days; thus, sampling errors arising from systematic diurnal variations may be averaged out at low latitudes. Local time coverage of the higher latitudes (greater than 30°) is not as complete (see Fig. 1). TRMM(12) has positive LW bias errors up to 7 W m^{-2} over much of the United States and Mexico, and similarly large negative errors over South America at latitudes south of 20°S. The location and magnitude of TRMM errors are also dependent on the satellite crossing time since different synoptic events may be sampled differently or entirely missed. For example, TRMM(00), not shown, has maximum positive errors over southern South America and large negative errors over North America. The LW errors are generally small over the oceans since low-level clouds tend to predominate. The LW sampling errors for EOS-AM and EOS-PM are also shown in Fig. 9. Each of the EOS orbits samples most regions within 2 h of noon and midnight, which captures the diurnal variations fairly well. There are notable exceptions in the western United States, in other scattered land regions, and in convection areas associated with the intertropical convergence zone (ITCZ) in the Pacific Ocean near 10°N.

Shortwave bias errors for the single satellites are given in Fig. 10. TRMM(12) has errors up to 25 W m^{-2} over both land and ocean regions due to the diurnal variations of cloud cover. The largest TRMM(12) errors are primarily located in the southern midlatitudes, while TRMM(00), not shown, has its greatest errors over a

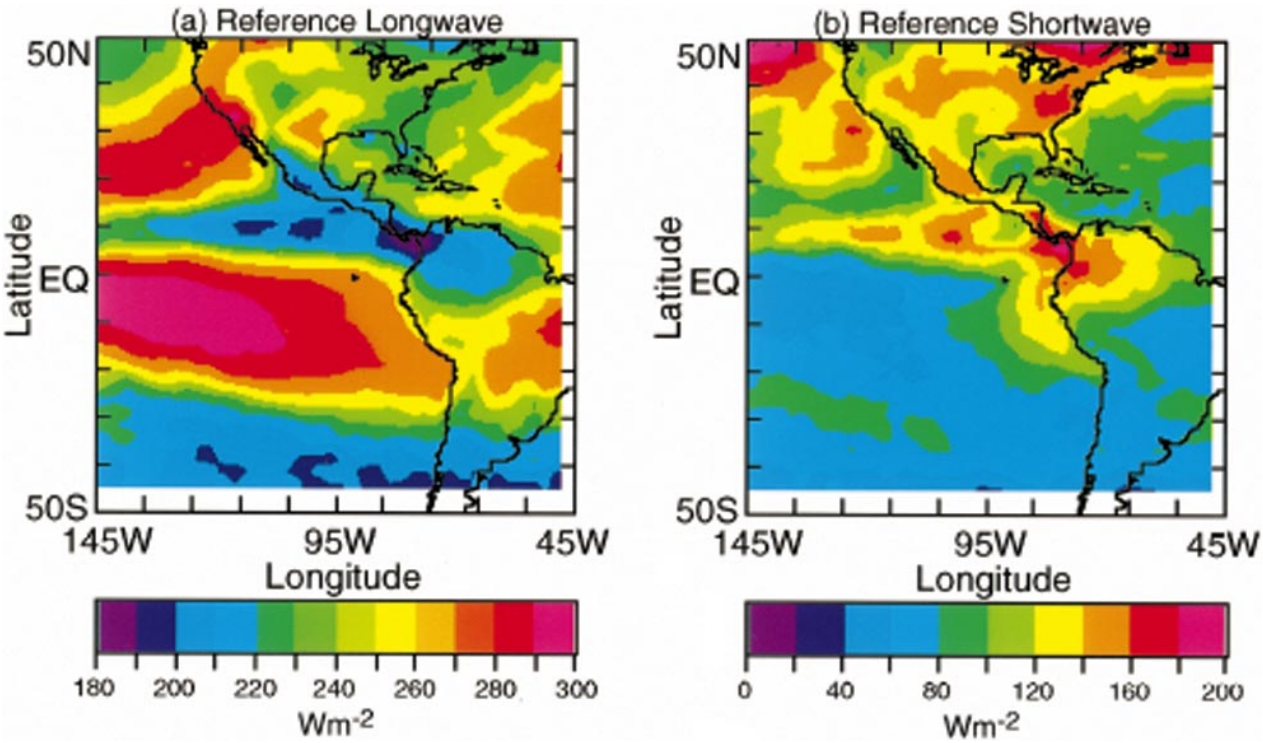

FIG. 8. GOES July 1985 reference (a) longwave and (b) shortwave data for ERB sampling studies.

large area between 20° and 40°N. EOS-AM and EOS-PM have SW bias errors of similar magnitude, but high errors are seen over a greater geographical area, mainly in the summer hemisphere.

For multiple satellites, the sampling times of the two individual satellites are simply combined before applying the ERBE-like TSA. Results for the two- and three-satellite combinations are given in Figs. 11 and 12 for LW and SW, respectively. The EOS–TRMM combinations use the TRMM(12) sampling; slightly different results can be expected for the other TRMM orbits. In every case, the two-satellite sampling error in the monthly mean is less than that of the single satellites. The combination of all three satellites reduces the error even more. Table 1 summarizes both the bias and rms errors for July and April 1985. The LW mean bias and rms errors are for land regions only, while SW errors are for the entire study region. For each case that includes a TRMM satellite, the range of values is given for all four TRMM starting times. For July 1985 (Table 1a), the magnitude of LW bias errors is less than 2 W m^{-2}. The LW rms error is from 3.9 to 5.0 W m^{-2} for TRMM; EOS-AM and EOS-PM errors are 2.9 and 2.6 W m^{-2}, respectively. Adding a second satellite reduces the rms error to 2.4 W m^{-2} or less, and the three-satellite combination error is smaller, 1.3–1.7 W m^{-2}.

In general, SW bias errors are somewhat greater than their LW counterparts. TRMM SW bias errors range from −1.7 to 3.1 W m^{-2}, while the EOS satellite SW bias is about −6 W m^{-2}. Adding a TRMM spacecraft to each of the EOS satellites decreases the bias to about −3.0 W m^{-2}; however, the combination of two EOS orbiters does not reduce the SW bias error. The three-satellite case bias errors vary from −3.4 to −4.0 W m^{-2}, similar to those for TRMM and one EOS satellite. The rms errors are about 10 W m^{-2} for single satellites, slightly less than 6 W m^{-2} for EOS plus TRMM cases, 7.8 W m^{-2} for the combination of two EOS satellites, and 4.9–5.4 W m^{-2} for the three-satellite case. For April 1985 (Table 1b), the bias and rms errors are generally smaller than for July; however, the trend of decreasing errors with an increasing number of satellites is essentially the same.

In summary, the ERBE time–space averaging algorithm gives regional monthly mean temporal sampling errors that are significantly reduced as more satellites are added. Satellites can fail prematurely; therefore, it is useful to provide a strategy to reduce time sampling errors, especially for the single satellite case. The TRMM satellite will be in orbit for a year before the launch of the first EOS satellite.

3. Method II: Geostationary-data-enhanced temporal interpolation

Method II incorporates 3-hourly geostationary radiance data to account for insufficiently sampled diurnal cycles. The key to this strategy is to use the narrowband (NB) geostationary data to assist in determining the shape of the diurnal cycle, but use the ERB broadband

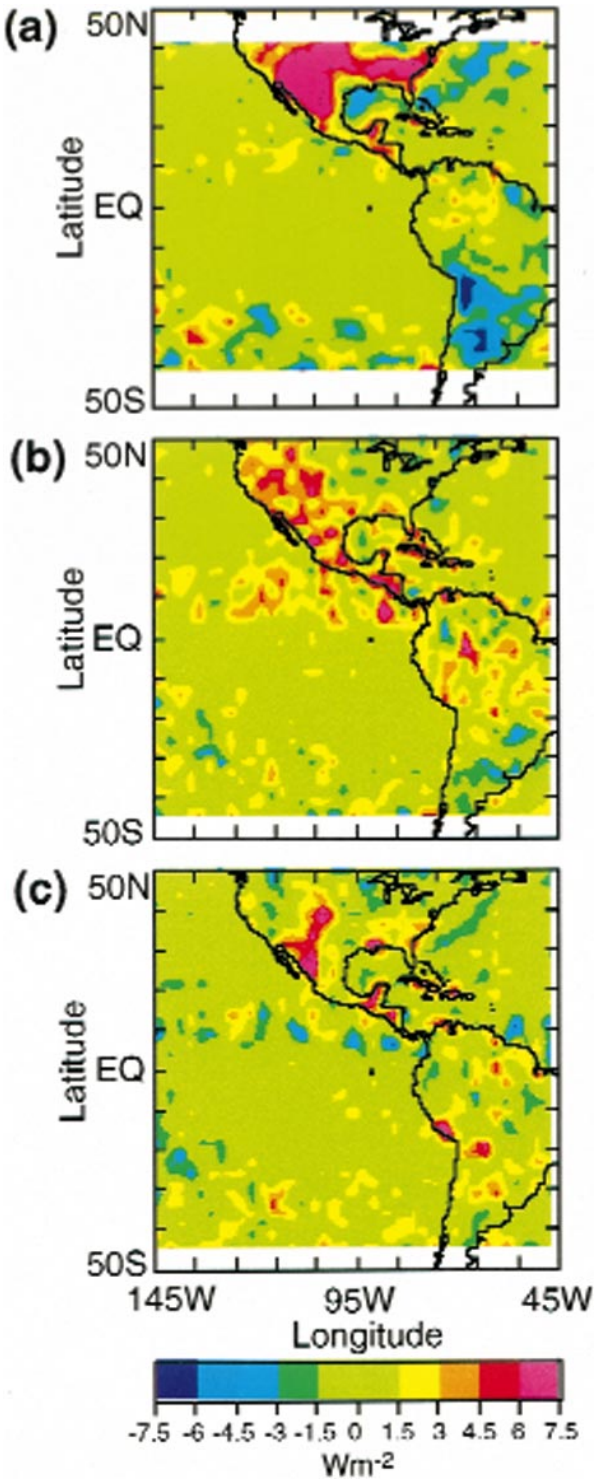

FIG. 9. Single satellite longwave bias errors for July using the ERBE TSA method for (a) TRMM, (b) EOS-AM, and (c) EOS-PM.

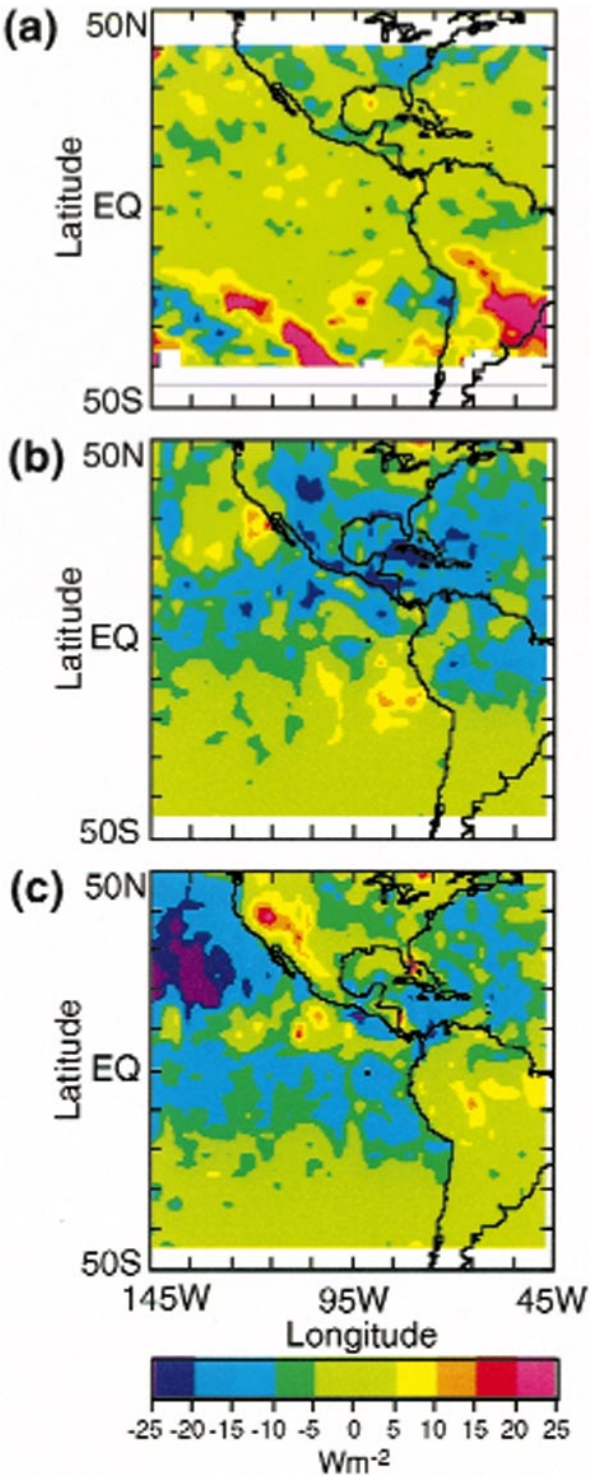

FIG. 10. Single satellite shortwave bias errors for July using the ERBE TSA method for (a) TRMM, (b) EOS-AM, and (c) EOS-PM.

(BB) satellite observations as the absolute reference to anchor the more poorly calibrated geostationary data. One advantage of this method is that it produces 3-hourly synoptic radiation fields for use in testing global models and for improved examination of the diurnal cycles of clouds and radiation.

The ERBE Science Team explicitly excluded the use of ancillary data in order to produce a self-contained,

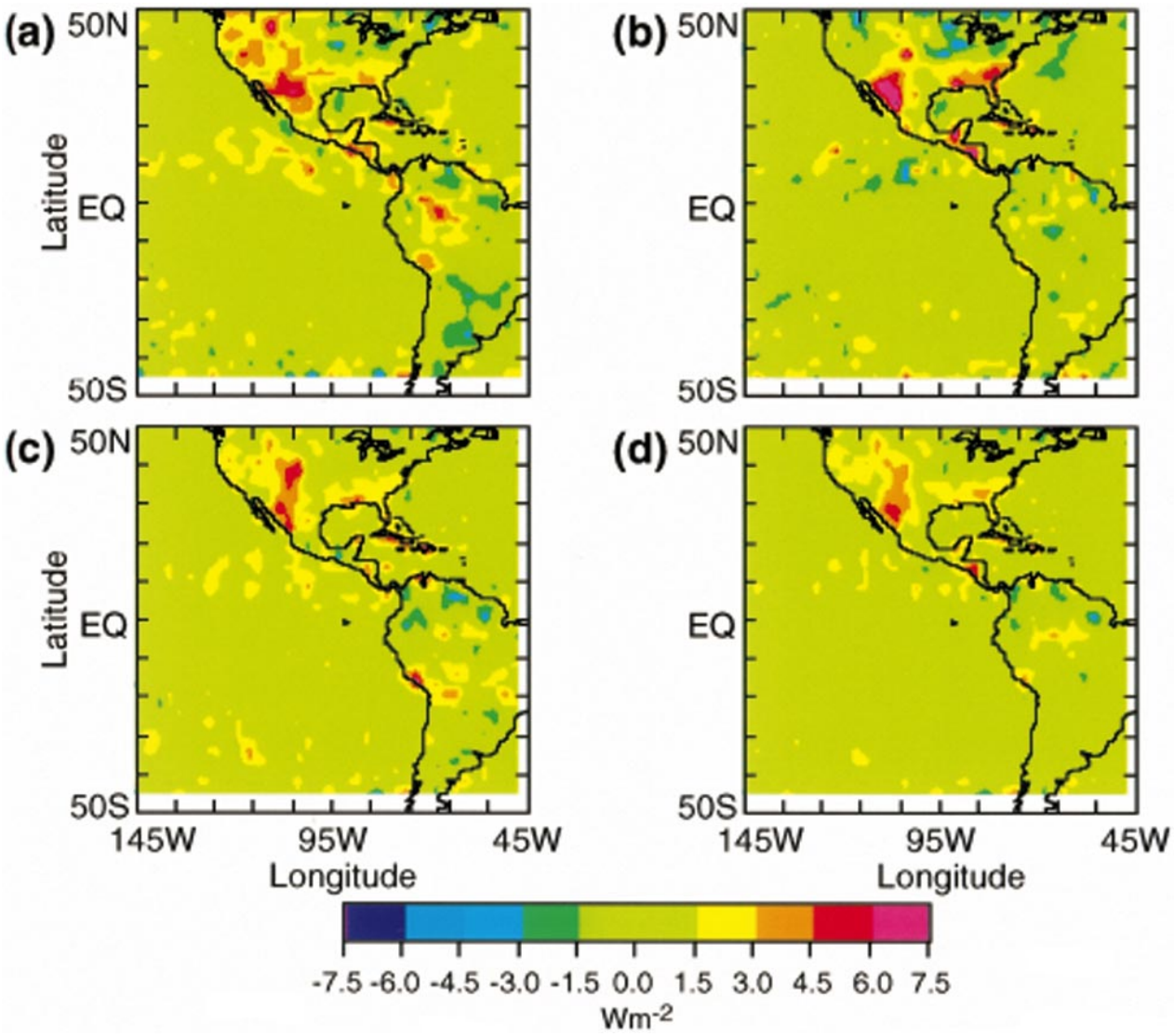

FIG. 11. Multiple satellite longwave bias errors for July using the ERBE TSA method for (a) EOS-AM + TRMM, (b) EOS-PM + TRMM, (c) EOS-AM + EOS-PM, and (d) EOS-AM + EOS-PM + TRMM.

consistent, and relatively straightforward climate dataset specifically geared toward accurate measures of monthly mean TOA fluxes. Significant improvements in time interpolation could be realized by using ancillary data to provide additional information concerning the meteorological changes occurring between ERB measurements.

Numerous simulations were performed to explore techniques for incorporating additional data sources into the time-averaging process. Because the main requirement of such data is to have enhanced temporal resolution, an obvious candidate data source is geostationary and polar-orbiting satellite radiance measurements. Geostationary data from such satellites as GOES, Meteosat, INSAT, and Geostationary Meteorological Satellite (GMS) provide measurements of NB visible and infrared radiances for much of the globe (approximately 50°N–50°S) at a temporal resolution as fine as every 30 min. The polar-orbiting satellites provide much less temporal information but are useful for providing information at higher latitudes.

Many attempts have been made to derive broadband radiation budget parameters from these narrowband measurements (Briegleb and Ramanathan 1982; Doelling et al. 1990; Minnis et al. 1991; Cheruy et al. 1991) because of the excellent temporal resolution of geostationary data. Generally, these and other studies (e.g., Gruber et al. 1994) have demonstrated that the narrowband measurements are insufficient for radiation budget calculations since they miss valuable spectral information contained in broadband observations. Minnis et al. (1991) showed that the longwave NB–BB relation varied significantly in time and

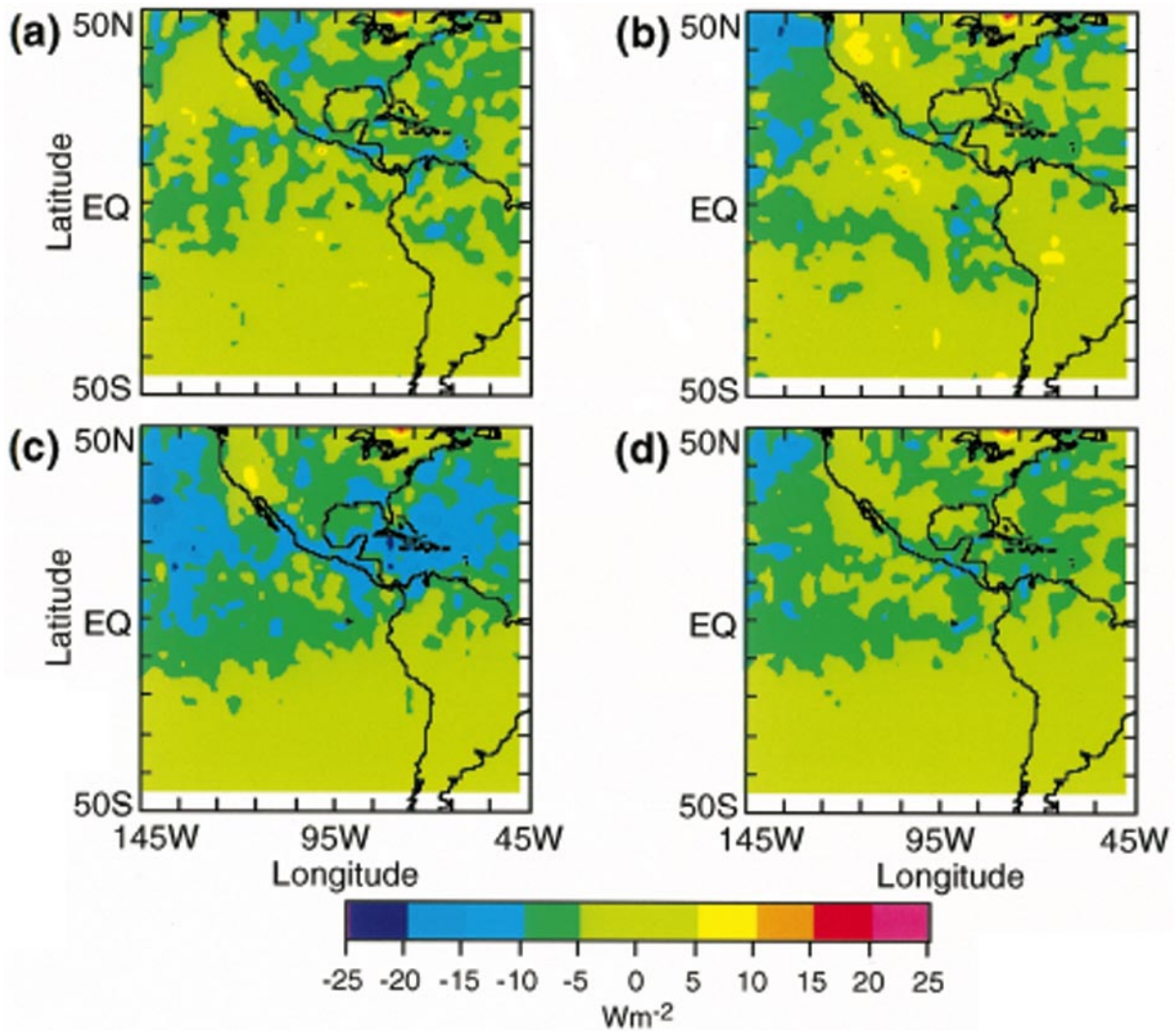

FIG. 12. Multiple satellite shortwave bias errors for July using the ERBE TSA method for (a) EOS-AM + TRMM, (b) EOS-PM + TRMM, (c) EOS-AM + EOS-PM, and (d) EOS-AM + EOS-PM + TRMM.

space even when water vapor, surface type, and cloud data were considered. Figure 13 shows regional means and standard deviations of the differences between ERBE-measured LW fluxes and broadband LW fluxes derived from GOES narrowband measurements for April 1985 using a global correlation that includes an atmospheric water vapor term. The overall rms error of the fit is approximately 11 W m^{-2}, and mean biases greater than 15 W m^{-2} are evident in many regions over the southeastern Pacific Ocean, over Colombia, and off the western coast of Mexico. The greatest standard deviations occur over the U.S.–Mexican border, the Amazon Basin, and the south-central Pacific. Regressions performed on a region-by-region basis can reduce the relative error to 7.7 W m^{-2} and essentially eliminate the mean bias. However, these regional correlations require frequent updating to account for changes in calibration and seasonal variations in the NB–BB relation. Thus, narrowband data should be used in climate studies only if the NB–BB relationship is continually calibrated using coincident measurements with a broadband ERB instrument. The techniques that produce the most accurate averages are described below.

a. Time interpolation of total-sky TOA LW flux

Instead of the combination of linear interpolation and idealized half-sine curves used by the ERBE-like technique to fit the observations, this method uses narrowband data to provide a more accurate picture of the shape of the curve that is fit to the observations.

The first step in the process is the conversion of the narrowband radiances into broadband fluxes using the regression techniques developed by Minnis et al. (1991). The regression is derived from coincident calibrated ge-

TABLE 1. Monthly error summary for ERBE-like diurnal averaging.

Satellite	Longwave (land only)		Shortwave (all regions)	
	Bias error (W m^{-2})	rms error (W m^{-2})	Bias error (W m^{-2})	rms error (W m^{-2})
(a) July 1985				
TRMM	−1.8–1.0	3.9–5.0	−1.7–3.1	8.2–11.1
EOS-AM	1.3	2.9	−6.0	9.7
EOS-PM	0.9	2.6	−5.9	9.6
EOS-AM + TRMM	0.0–0.8	2.0–2.4	−3.4–−2.4	5.0–6.0
EOS-PM + TRMM	−0.2–0.5	1.5–2.2	−3.3–−2.8	5.5–6.0
EOS-AM + EOS-PM	0.6	1.9	−6.1	7.8
EOS-AM + EOS-PM + TRMM	0.2–0.6	1.3–1.7	−4.0–−3.4	4.9–5.4
(b) April 1985				
TRMM	−1.4–1.1	2.3–5.5	−0.9–1.2	8.4–11.1
EOS-AM	0.9	2.7	−0.5	6.4
EOS-PM	0.4	2.3	−1.8	5.7
EOS-AM + TRMM	0.2–0.5	1.5–1.8	−0.1	3.7–4.3
EOS-PM + TRMM	−0.1–0.1	1.5–1.8	−1.0–−0.5	3.6–4.0
EOS-AM + EOS-PM	0.1	1.7	−1.2	3.6
EOS-AM + EOS-PM + TRMM	0.1	1.1–1.2	−0.7–−0.5	2.6–2.8

ostationary and ERB measurements and ancillary relative humidity data. The form of the regression is

$$F_{\mathrm{FNB}} = a_0 + a_1 F_{\mathrm{NB}} + a_2 F_{\mathrm{NB}}^2 + a_3 F_{\mathrm{NB}} \ln(\mathrm{rh}), \quad (8)$$

where F_{FNB} is the LW broadband flux derived from the narrowband, F_{NB} is the narrowband flux, rh is the column-averaged relative humidity, and a_i are the derived coefficients. The LW narrowband flux is derived from the narrowband radiance using

$$F_{\mathrm{NB}} = 6.18\gamma(\theta) I_{\mathrm{NB}}, \quad (9)$$

where I_{NB} is the LW narrowband radiance, $\gamma(\theta)$ is the LW limb-darkening function at viewing zenith angle θ, and 6.18 represents the product of the limb-darkening function integrated over an entire hemisphere and the narrowband spectral interval (Minnis et al. 1991).

To account for temporal variability in the regressions, new coefficients are derived for each month using data

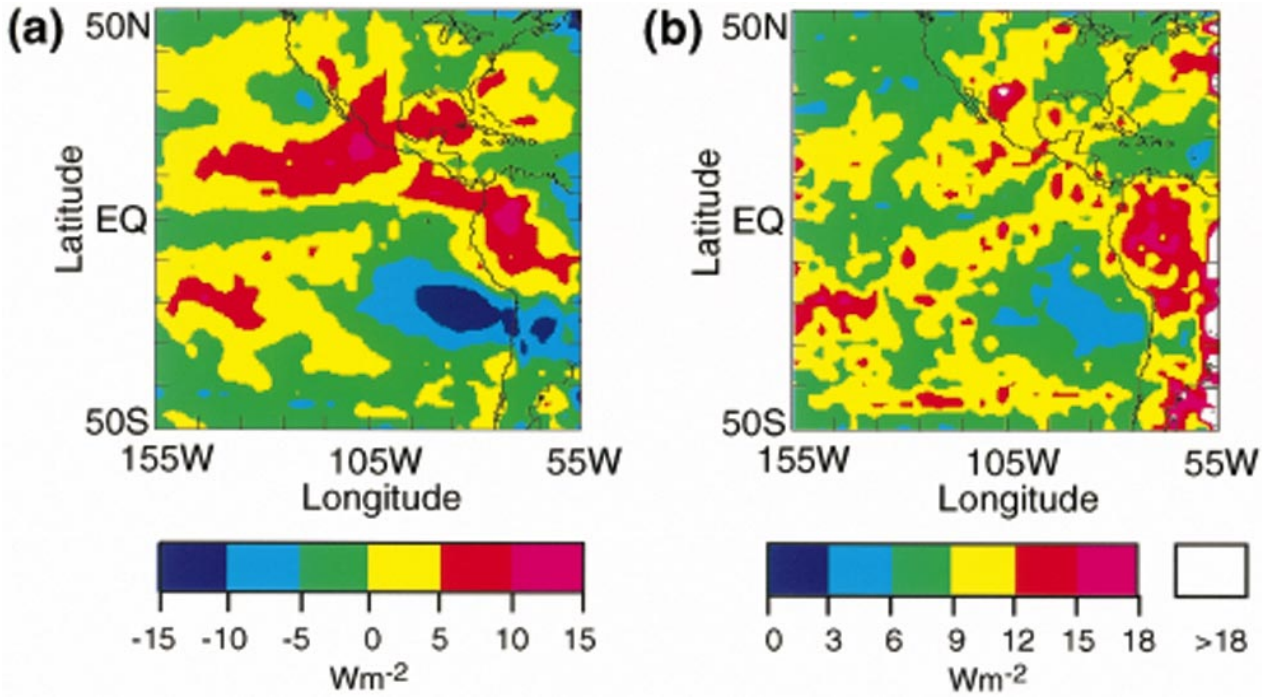

FIG. 13. (a) Regional means and (b) standard deviations of the differences between ERBE-measured LW fluxes and broadband fluxes derived from GOES narrowband measurements for April 1985.

from all regions in the satellite field of view. Separate correlations are derived for each of the five ERBE geographical scene types. The derivation of separate regressions for individual regions in order to account for spatial variability is not feasible for CERES. This is accomplished instead by normalizing the broadband fluxes derived from the narrowband data to the most recently observed LW measurement.

Once an estimate of broadband flux has been made from each narrowband measurement, a complete series of F_{FNB} is constructed by using the ERBE-like interpolation technique. A normalization ratio, ε, is then defined at the time of each LW measurement during the month:

$$\varepsilon(t_0) = \frac{F_{\mathrm{BB}}(t_0)}{F_{\mathrm{FNB}}(t_0)}, \tag{10}$$

where t_0 is the time of the LW broadband measurement, F_{FNB} is the LW from narrowband after global regression, and F_{BB} is the longwave BB measurement. This ratio is linearly interpolated to all hours of the month. Final values of F_{BB} for all hours between the observations are calculated by multiplying F_{FNB} by the normalization ratio ε for that hour. Although there may be some spatial mismatch in the ratioed NB and BB data, this renormalization is sufficient to reduce the residual regional variance from the NB–BB regression. The LW normalization process ensures that the final diurnal variability assumed in the time interpolation process is directly tied to the measured fluxes. Errors incurred by variations in the calibration of the narrowband instruments are also reduced. The narrowband data are used to provide extra information concerning meteorological variations between the measurements. As more than one ERB instrument becomes operational, the reliance on the narrowband data to provide the diurnal shape will diminish. With the improved time sampling, the interpolated curves will be dominated by the observed fluxes.

Several studies have been performed to demonstrate the benefits of incorporating narrowband measurements into the averaging process. Past studies have shown that the use of techniques, such as the half-sine fit used by ERBE over land regions, is more effective than linear interpolation in reproducing the LW diurnal variability seen in narrowband measurements (Brooks and Minnis 1984a). Studies such as these rely on using 1-hourly GOES data converted to broadband flux using NB–BB regressions as a reference dataset. The effects of sampling patterns and the relative errors inherent to various interpolation schemes can be evaluated by sampling this reference set and comparing the results of the interpolation with the reference set.

To show the improvement in interpolation using this geostationary-data-enhanced method, it is necessary to have three independent datasets: the broadband measurements, the narrowband time series, and an additional broadband reference dataset. Since the GOES data are used in the averaging process, it is improper to use GOES as the reference dataset. In addition, there is no 1-hourly global broadband dataset to use as the truth.

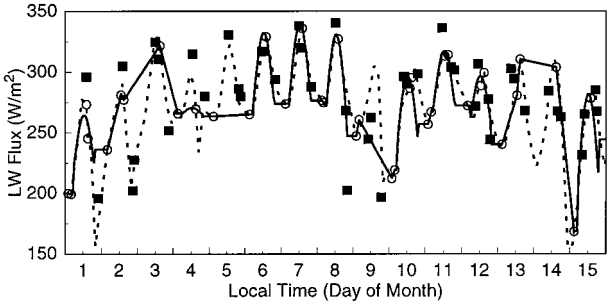

FIG. 14. Time series of ERBE ERBS (filled squares) and *NOAA-9* (open circles) LW flux observations and interpolated values from July 1985 over New Mexico. The *NOAA-9* data are interpolated to other hours and compared to the observed values from ERBS. The solid curve shows ERBE time interpolation values; the dashed line shows the geostationary-data-enhanced interpolation.

This problem is overcome by using ERBE data from two different satellites, ERBS and *NOAA-9*, as two independent datasets. Observations from one satellite are interpolated to the observation times of the other using four different techniques (denoted as techniques a–d). Technique a is the ERBE-like combination of linear and half-sine interpolation. Techniques b, c, and d are geostationary-data-enhanced methods. The first, b, uses 1-hourly GOES data as a best-case test. The second technique, c, uses the 3-hourly time sampling that is most likely to be available during CERES processing. Finally, in technique d, ERBE measurements are predicted simply using the 3-hourly narrowband measurements converted to broadband using the regression fit but without the normalization to ERBE to account for regional variations. This method is included to determine the need for continually anchoring the narrowband-derived fluxes to the measurements.

A comparison of two of these techniques, a and c, is displayed in Fig. 14 for an ERBE 2.5° region over New Mexico during the first 15 days of July 1985. The solid curve represents the ERBE-like technique a, while the dashed line is the normalized 3-hourly narrowband shapes technique c. ERBS observations of TOA LW flux are displayed as solid squares and *NOAA-9* observations are open circles. The interpolation techniques are applied to the *NOAA-9* data in order to predict the ERBS observations. Both techniques perform well when sampling is adequate and cloudiness is constant as found during days 6–8 and 10–12. However, the ERBE TSA severely misses several nighttime points during days 1–3, as well as daytime points on days 6 and 14. Technique c does a much improved job of filling in the fluxes in the hours between the observations. In particular, the predicted daytime fluxes on day 5 and the nighttime fluxes on days 1–4 are closer to the ERBS values. A few ERBS fluxes were missed because of the 3-h time

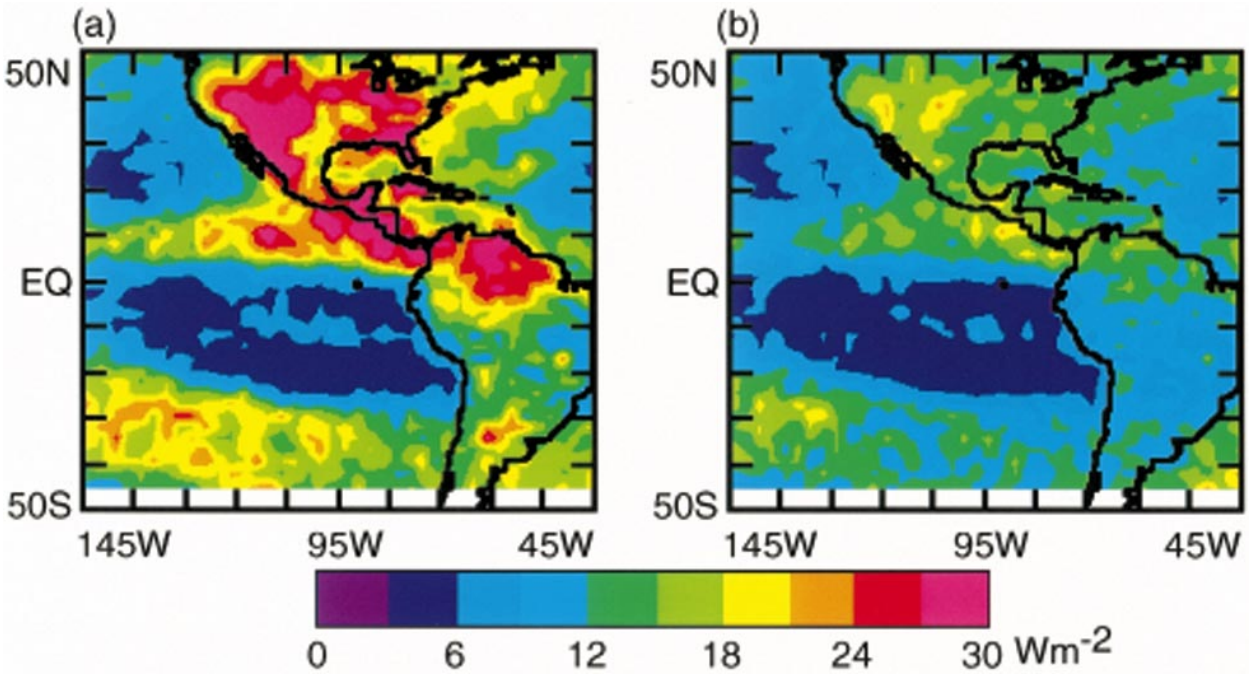

FIG. 15. Regional comparison of instantaneous longwave interpolation errors for (a) ERBE-like and (b) geostationary-data-enhanced time interpolation methods for July 1985.

resolution of the narrowband data, but, overall, technique c shows substantial improvement over technique a.

Figure 15 compares the geographical distribution of the LW rms interpolation errors for the ERBE-like (left panel) and geostationary-data-enhanced (right panel) temporal interpolation methods for July 1985. Technique c reduced the ERBE mean instantaneous interpolation rms errors by 50% for both LW and SW (not shown). The greatest improvement using the CERES technique occurs in regions with pronounced diurnal cycles in clouds such as the ITCZ and the convective regions of North and South America.

TABLE 2. Comparison of LW flux time interpolation techniques using ERBE data from (a) July 1985 and (b) April 1985. Instantaneous mean and rms differences (W m^{-2}) between *NOAA-9* LW flux measurements and fluxes predicted from ERBS observations.

	NOAA-9 mean flux	Total error		Time interpolation error	
		mean	rms	mean	rms
(a) July 1985					
Coincident data	243.6	2.4	10.6	—	—
a: ERBE TSA	246.5	2.8	16.9	0.4	13.2
b: With 1-hourly GOES	246.5	3.1	11.4	0.7	4.2
c: With 3-hourly GOES	246.5	2.8	12.0	0.4	5.6
d: Nonnormalized/3 h	246.5	2.6	14.4	0.2	9.7
(b) April 1985					
Coincident data	246.6	−0.1	10.0	—	—
a: ERBE TSA	246.2	0.7	15.7	0.8	12.1
b: With 1-hourly GOES	246.2	0.8	11.3	0.8	5.3
c: With 3-hourly GOES	246.2	0.7	11.8	0.7	6.3
d: Nonnormalized/3 h	246.2	0.2	14.9	0.2	11.0

The results for the four interpolation techniques are summarized in Table 2 for all 2.5° regions between 50°N–45°S latitude and 155°–55°W longitude during the month of July 1985 and between 50°N–45°S latitude and 145°–45°W longitude during April 1985. The first row of the table contains a comparison of coincident ERBS and *NOAA-9* ERBE observations. Data from all regions viewed by both ERBE instruments during the same hour are included. Since this comparison is performed using data averaged in coincident hour boxes, any difference between the two can be due to a combination of temporal and spatial variations within the 2.5° region over 1 h as well as miscalibration between the two instruments or errors in the ADMs used to convert the radiances to fluxes. There is a 2.4 W m^{-2} bias and 10.6 W m^{-2} instantaneous rms error (difference) between the two datasets in July. The April data show similar values of -0.1 ± 10.0 W m^{-2}. An estimate can be made of the magnitude of the errors due to the ADMs. When the two instruments view the scene with viewing zenith angles within 10° of each other, the rms differences are reduced to 5–6 W m^{-2} for both months, while the biases remain unchanged.

Although the overall *NOAA-9*–ERBS biases are small (less than 1% of the mean flux), they are significant to this study. The results of the various time interpolation schemes must be compared with these coincident biases. A perfect time interpolation should not produce a zero

bias, but rather should reproduce the bias in the coincident ERBS and *NOAA-9* data.

The successive rows of Table 2 show the capability of each interpolation technique to reproduce the *NOAA-9* observations by temporally interpolating the ERBS data. The mean LW flux from *NOAA-9* is provided in column 1. The next two columns contain the absolute instantaneous mean and rms difference between the observed *NOAA-9* flux and the flux predicted for that hour by interpolating the ERBS observations. Estimates of the mean and rms error from the time interpolation processes have also been included in columns 4 and 5. The rms due to time interpolation, rms_{t_i}, is calculated assuming that the time interpolation error is independent of the rms difference between coincident ERBS and *NOAA-9* measurements, rms_0. It is calculated as

$$\text{rms}_{t_i}^2 = \text{rms}_T^2 - \text{rms}_0^2, \tag{11}$$

where rms_T is the total rms from the technique. The mean time interpolation error is simply the difference of the total mean error and the mean difference in the coincident fluxes.

The lowest rms errors are obtained using narrowband data with 1-h temporal resolution. However, there is only a slight overall (1–2 W m^{-2}) degradation in the rms error when 3-hourly data are used. Although this degradation is somewhat greater in certain cloud regimes, there is a substantial improvement in the time interpolation error using the GOES data over the ERBE time-averaging scheme. The rms error due to time interpolation decreases from 13.2 to only 5.6 W m^{-2} for the July data and from 12.1 to 6.3 W m^{-2} for April. In addition, the mean bias is less than 1 W m^{-2} for all cases.

Clearly, the renormalization process is necessary for accurate temporal interpolation. Technique d simply used the global NB–BB correlations to produce the LW flux time series from the GOES data. Compared to technique c, it increases the instantaneous time interpolation rms error from 5.6 to 9.7 W m^{-2} in July and from 6.3 to 11.0 W m^{-2} in April. The latter error is only a minimal improvement over the ERBE-like technique a. Through renormalization, the time series of LW flux is accurately tied to the original observations. Region-to-region variations in the NB–BB correlations and temporal variations in the narrowband calibration are explicitly taken into account.

The statistics from the above simulations show that the geostationary-data-enhanced technique improves the instantaneous flux estimates. It is also crucial that the time interpolation technique for instantaneous flux does not adversely affect the monthly means. Harrison et al. (1990) demonstrated that ERBE regional monthly mean LW flux estimates are accurate within 1 W m^{-2} if data from two satellites are used. For July, over the entire GOES region, the ERBE technique a produces monthly mean flux averaged over all regions of 249.0 W m^{-2}. For techniques c and d, the averages are 248.8 and 248.4 W m^{-2}, respectively. In all three cases, the rms of the regional time interpolation error in the monthly mean is less than 2 W m^{-2}. Thus, the enhancements to the interpolation process are not adversely affecting the monthly means. Once again, the anchoring of the LW fluxes to the observations in technique c produces an improvement over the results of technique d.

Sampling effects are also minimized when narrowband data are used in the interpolations. The differences in regional monthly mean fluxes calculated using the two ERBE instruments demonstrate the sampling impact. The polar-orbiting *NOAA-9* satellite produces ERBE sampling near 0230 and 1430 LST throughout the month. The local time of observations from the precessing ERBS satellite slowly changes during the month. The region-to-region rms difference between the monthly mean estimates from the two satellites is a measure of independence of the interpolation from sampling effects. During April, when the mean difference between the two datasets is nearly zero, the regional rms difference in monthly mean is 2.4 W m^{-2} for technique a and 1.7 W m^{-2} for technique c. As expected, incorporating the narrowband data time series increased the accuracy of filling in flux values for times between measurements.

b. Time interpolation of clear-sky TOA LW flux

The ERBE-like averaging technique does not yield clear-sky flux estimates for all hours of the month. The relative scarcity of clear-sky flux estimates derived from ERBE data necessitated the use of monthly–hourly fits instead of continuous interpolation. CERES is geared toward studying the effects of clouds on the earth's radiation budget, so there will be a significant improvement in the quality of clear-sky data. The frequency of clear scenes misclassified as partly cloudy will be substantially reduced.

Because of these improvements to the clear-sky dataset, time interpolation of clear-sky LW flux is performed in a manner identical to the total-sky product. The main information provided by the narrowband geostationary data relates to changes in meteorology and cloudiness. For clear skies, the idealized ERBE models work well. If no clear-sky measurements are available on a given day, clear-sky fits from the nearest day with data is used.

c. Time interpolation of total-sky TOA SW flux

There are several major challenges that must be addressed when developing a method of incorporating narrowband data into the process of temporal interpolation of TOA SW fluxes. First, in order to calculate a narrowband albedo, anisotropic effects must be removed through the use of bidirectional reflectance models. Since these models are functions of both surface type and cloud cover, it is important to have accurate esti-

mates of the cloud amount at the times of the narrowband observations. Second, the narrowband albedos must be converted into equivalent broadband values. As with the TOA LW flux, a normalization process is used to ensure that the resulting time series of albedos is tied to the broadband observations.

Two methods are used to determine broadband albedo from narrowband reflectances. The first method (referred to as the GOES cloud method) uses cloud information derived from the narrowband data. For this study, the cloud parameters were derived using the Hybrid Bispectral Threshold Method (HBTM) of Minnis et al. (1987). Each narrowband pixel is classified as either clear or cloudy. For each region, these pixels can be averaged to produce the cloud amount (cld) and separate estimates of clear sky (r_{clr}) and overcast (r_{cld}) reflectance. Narrowband albedo, α_{nb}, can then be computed from r_{clr} and r_{cld} using

$$\alpha_{nb} = \frac{(1.0 - \text{cld})(r_{clr})}{R_{clr}} + \frac{(\text{cld})(r_{cld})}{R_{ovc}}, \qquad (12)$$

where r is narrowband reflectance ($r = I_{nb}/S_v$), cld is the narrowband cloud amount, and R is the bidirectional anisotropic factor. Here, I_{nb} is the mean observed narrowband VIS radiance and S_v is the earth–sun distance-corrected narrowband solar constant (nominal value for GOES of 526.9 W m^{-2} sr^{-1} μm^{-1}).

The second method (referred to as the ERBE cloud method) assumes that no cloud information is derived from narrowband data. The only available cloud information is the scene fractions of the four ERBE cloud classifications measured at the times of the broadband observations. Cloud amount at the time of the narrowband measurement is estimated by linearly interpolating these scene fractions. However, there is still insufficient information to calculate narrowband albedos since there are not separate estimates of reflectance for each cloud classification. A composite bidirectional anisotropic factor can be calculated by weighting the individual factors by both the scene fraction and the relative amount of energy reflected by each cloud classification. To do this, initial estimates of albedo (α_i) are calculated at the narrowband times by using the ERBE interpolation technique described in Eq. (4). The narrowband radiances can then be converted to narrowband albedos using

$$\alpha_{nb} = (I_{nb}/S_v) \Bigg/ \left(\sum_{i=1}^{4} R_i \alpha_i f_i \Bigg/ \sum_{i=1}^{4} \alpha_i f_i \right), \qquad (13)$$

where f_i and R_i are the ERBE scene fraction and bidirectional anisotropic factors for ADM class i interpolated to the time of the narrowband data.

Broadband anisotropic factors have been used in the above calculation. Doelling et al. (1990) showed that the use of ERBE broadband anisotropic factors in the calculation of albedos from GOES measurements did not degrade the regressions between GOES and ERBE albedos.

For both the GOES and ERBE cloud methods, the narrowband albedos are converted to estimates of broadband albedos using regressions of the form used by Doelling et al. (1990),

$$\alpha_{BB} = b_0 + b_1 \alpha_{NB} + b_2 \alpha_{NB}^2 + b_3 \ln[\sec(\theta_0)], \qquad (14)$$

where α_{NB} is the narrowband albedo, α_{BB} is the broadband albedo estimate from the narrowband data, and θ_0 is the solar zenith angle at the center of the region at the synoptic time. Separate regressions have been performed for each of the five ERBE geographical scene types.

A time series of broadband albedos calculated from narrowband measurements in the above manner can still contain significant errors (see Doelling et al. 1990; Briegleb and Ramanathan 1982). Doelling et al. (1990) found that regressions of the form in (14) have rms regression errors in excess of 14%. In addition, they showed that the relationship can vary substantially from region to region. The best measurements of broadband SW flux are those derived from broadband ERB instruments. Like the LW methods, the time series of narrowband measurements should serve only as a guide for tracking changes in cloudiness between the ERB observation times. This can be significant since variations in cloudiness have a much greater impact on the SW. A change from a 100% clear scene to 100% overcast may result in a decrease in LW flux of 20%–30%, but total-scene albedo may increase by 400%–500%.

As with the LW, the derived albedos are normalized to the broadband observations. At each SW observation time, a normalization ratio can be defined as the ratio of the observed albedo to α_{BB}. This ratio can then be interpolated to all daylight hours and used to normalize each estimate of α_{BB}. However, it has been found that due to the large variation of albedo with cloud amount, normalization at all hours can produce albedos outside of physical limits; constraints need to be determined in order to normalize more hour boxes. For this study, albedos are normalized only for a 2-h window surrounding each SW measurement. Because of the variability of the SW narrowband–broadband relationship, even this limited normalization process produces a more accurate interpolation.

The accuracy of these techniques was tested using ERBE ERBS and *NOAA-9* SW data. Measurements from ERBS were used to predict SW flux values measured from *NOAA-9* using five techniques. Technique a uses the ERBE method. The other techniques employ narrowband SW radiances from GOES. The difference between the techniques is in the cloud data used to select the ADMs necessary to convert the narrowband radiances into fluxes. The interpolation is first performed using cloud amounts and cloud and clear albedos derived from the narrowband data using HBTM (Minnis et al. 1987). The results from this technique represent best-case examples and are labeled b and c when applied to 1-hourly and 3-hourly GOES data, respectively. The

TABLE 3. Comparison of SW flux time interpolation techniques using ERBE data from (a) July 1985 and (b) April 1985. Instantaneous mean and rms differences (W m^{-2}) between *NOAA-9* SW flux measurements and fluxes predicted from ERBS observations.

	NOAA-9 mean flux	Total error		Time interpolation error	
		mean	rms	mean	rms
(a) July 1985					
Coincident data	259.4	5.2	36.5	—	—
a: ERBE TSA	228.5	0.0	53.8	−4.6	43.1
b: With 1-hourly GOES + GOES clouds	228.5	−1.0	35.1	−5.6	14.1
c: With 3-hourly GOES + GOES clouds	228.5	−0.8	36.0	−5.4	16.2
d: With 1-hourly GOES + ERBE clouds	228.5	6.2	39.5	1.6	22.9
e: With 3-hourly GOES + ERBE clouds	228.5	5.9	39.6	1.4	23.1
f: Nonnormalized 3 h + ERBE clouds	228.5	7.1	42.5	2.5	27.8
(b) April 1985					
Coincident data	251.0	5.1	39.1	—	—
a: ERBE TSA	233.3	1.7	55.1	−3.0	41.4
b: With 1-hourly GOES + GOES clouds	233.3	5.7	37.1	1.0	7.5
c: With 3-hourly GOES + GOES clouds	233.3	3.4	38.5	−1.3	12.7
d: With 1-hourly GOES + ERBE clouds	233.3	5.2	39.9	0.4	16.5
e: With 3-hourly GOES + ERBE clouds	233.3	3.2	42.4	−1.5	21.8
f: Nonnormalized 3 h + ERBE clouds	233.3	3.1	44.9	−1.6	26.4

next two techniques, d and e, use linearly interpolated ERBE cloud amounts and albedos to select the proper anisotropic factor. Technique d uses 1-hourly GOES data; technique e uses 3-hourly data. A final technique, f, is identical to e, but it does not include the renormalization of the narrowband-derived fluxes to the nearest observation.

The results are shown in Table 3. There is a significant bias between coincident ERBS and *NOAA-9* measurements. During both July and April, the instantaneous mean differences are approximately 5.2 W m^{-2} with approximately 38 W m^{-2} rms. These differences are much larger than the corresponding values associated with the LW flux. This is due to the greater dependence on ADMs for deriving SW flux from the observations. When the coincident comparison is limited to times when both instruments are viewing within 20° of nadir, the mean bias in July is −1.4 W m^{-2} and the rms difference falls to only 13.1 W m^{-2}, which is of the same magnitude as the LW. Unfortunately, the additional errors associated with model selection hamper some of the comparisons in the simulations. Since the mean differences of even coincident data are strongly angle dependent, it is difficult to determine the absolute accuracy of the averaging techniques. However, the relative effectiveness of the methods can be measured by comparing the rms errors. Thus, analysis of the simulations will stress a comparison of the instantaneous rms errors, not the biases.

The mean and rms errors due to time interpolation are calculated in a slightly different fashion than that used for the LW flux simulations. As seen in Table 3, the mean SW flux for the coincident data is 20–30 W m^{-2} greater than the mean fluxes used in the time interpolation. There are fewer (approximately 7000) coincident data points as compared with the approximately 35 000 *NOAA-9* measurements that can be predicted from ERBS data. The difference in the mean fluxes occurs because the coincident data occur at a lower average solar zenith angle. To accommodate this difference, the rms errors from the coincident data [rms_0 from (11)] are first linearly scaled by the ratio of the fluxes before being subtracted from the total rms errors.

The addition of narrowband data significantly decreases the interpolation rms errors. As explained above, the ERBE time interpolation technique necessarily assumes constant cloudiness over each day for which there is only one time of observation. By introducing information concerning the temporal variation in cloudiness through the addition of narrowband data, the time interpolation error has been reduced from 43.1 W m^{-2} to less than 28 W m^{-2} in all cases b–f for the July data. The reasons for this increased accuracy can be seen in Fig. 16, which shows 3 days of SW albedo measured by ERBE during July 1985 in the same region in New Mexico as in Fig. 14. The ERBS observations are shown as black squares. The *NOAA-9* observations are open circles. Also shown are the results of interpolations using the *NOAA-9* data and the ERBE time interpolation technique a and the 3-hourly geostationary data technique e. During the first two days, the cloudiness remained constant throughout the day and the two techniques produce similar results. On the third day, however, there was apparently a shift in cloudiness between ERBS and *NOAA-9* observation times. The ERBE time interpolation technique severely overestimates the albedo over most of the day. The GOES data, however, provide the means for correctly modeling the albedo on that day.

Technique e provides a definite improvement over the ERBE technique, reducing the rms time interpolation error from 43.1 to 23.1 W m^{-2} in July and from 41.4 to 21.8 W m^{-2} in April. The bias errors also show improvement. As expected, the mean rms error associated

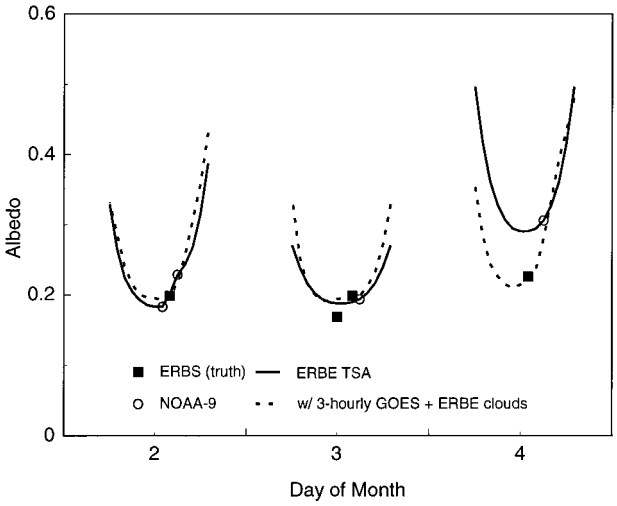

FIG. 16. Time series of ERBE ERBS (filled squares) and *NOAA-9* (open circles) SW albedo observations and interpolated values from July 1985 over New Mexico. The solid curve shows the ERBE time interpolated values; the dashed curve shows the geostationary-data-enhanced interpolation.

with using 1-hourly data in technique d shows a slight improvement over using 3-hourly data. However, this improvement is small compared to the advantages of data volume reduction if 3-hourly data are used instead. Furthermore, when generating SW flux estimates for synoptic maps, the difference between the 1- and 3-hourly data is not significant. Since the fluxes will be derived at times of geostationary observations, the errors should be closer to the 1-hourly estimates shown here. It is clear in these results that the renormalization of the SW flux estimates to the nearest observation is important. The rms errors increase by 4–5 W m^{-2} when this renormalization is not included in technique f.

An additional improvement is seen if cloud information is derived at the times of geostationary measurements. As stated above, errors can be quite large from improper selection of SW ADMs due to misclassification of cloud amount. Increasing the accuracy of cloud parameters should, therefore, decrease errors in the NB–BB conversion of the GOES data. For techniques d–f, cloud fraction estimates are derived at each hour by linearly interpolating between ERBE observations. Cloud fractions derived directly from the narrowband data should be more accurate since time interpolation of cloud fraction is no longer necessary.

The results of using this improved cloud information are shown in techniques b and c for 1- and 3-h GOES data, respectively. For the 3-hourly case, rms interpolation errors decrease by 7–9 W m^{-2} from technique e, which uses the ERBE cloud information. Part of this error is due to the linear interpolation of cloud fractions, but some of the error is due to incorrect ERBE scene identification. This latter error should be greatly diminished because of the improved cloud data from future ERB experiments such as CERES. Thus, the improvement of technique c over e should not be as great for CERES. The actual gain in accuracy using c instead of e for CERES needs further study.

These new temporal interpolation methods are aimed at improving instantaneous estimates of flux. It is important to ensure that the estimates of monthly mean flux are not adversely affected. ERBE produced regional monthly mean SW flux estimates to within 3 W m^{-2} (Harrison et al. 1990). For July, the ERBE method a produces monthly mean flux averaged over all regions of 95.1 W m^{-2}. For techniques e and f, the averages are 95.5 and 95.6 W m^{-2}, respectively. Thus, the enhancements to the interpolation process are not adversely affecting the monthly means. Once again, anchoring the SW fluxes to the observations in technique e produces an improvement over the results of technique f.

d. Time interpolation of clear-sky TOA SW flux

As is the case for the clear-sky LW flux, there should be a more accurate determination of clear-sky SW data with the CERES experiments than with ERBE. The ERB data are interpolated using the clear-sky ADMs appropriate to the regional surface type. Thus, geostationary data should not be needed for clear-sky modeling. The main information provided by the narrowband data is the changes in meteorology and cloudiness. For clear skies, the available directional models should work well for time interpolation. Geostationary data could only be used in the processing of clear-sky data if separate total-sky and clear-sky narrowband radiances are derived from the narrowband measurements.

4. Conclusions

Two general methods are presented and evaluated for temporally interpolating ERB measurements to compute averages of TOA SW and LW flux. A method similar to that used by the ERBE yields good monthly averages, but it does not always provide an accurate representation of diurnal variations. The new CERES geostationary-data-enhanced technique incorporates high-temporal resolution data from geostationary satellites and reduces the ERBE-like mean instantaneous interpolation rms errors by 50% for both SW and LW. The greatest improvement using the geostationary-data-enhanced technique occurs in regions with pronounced diurnal cycles in clouds, such as the ITCZ and the convective regions of North and South America. While proposed for application to future earth radiation budget measurement programs such as CERES, these new techniques may also be useful for improving the fluxes derived from earlier ERB data.

REFERENCES

Barkstrom, B. R., 1984: The Earth Radiation Budget Experiment (ERBE). *Bull. Amer. Meteor. Soc.,* **65,** 1170–1185.

——, and G. L. Smith, 1986: The Earth Radiation Budget Experiment: Science and implementation. *Rev. Geophys.,* **24,** 379–390.

——, E. F. Harrison, R. B. Lee III, and the ERBE Science Team, 1990: Earth Radiation Budget Experiment, preliminary seasonal results. *Eos, Trans., Amer. Geophys. Union,* **71,** 297–305.

Briegleb, B. P., and V. Ramanathan, 1982: Spectral and diurnal variations in clear sky planetary albedo. *J. Climate Appl. Meteor.,* **21,** 1168–1171.

Brooks, D. R., and P. Minnis, 1984a: Comparison of longwave diurnal models applied to simulations of the Earth Radiation Budget Experiment. *J. Climate Appl. Meteor.,* **23,** 156–160.

——, and ——, 1984b: Simulation of the earth's monthly average regional radiation balance derived from satellite measurements. *J. Climate Appl. Meteor.,* **23,** 392–403.

——, E. F. Harrison, P. Minnis, J. T. Suttles, and R. S. Kandel, 1986: Development of algorithms for understanding the temporal and spatial variability of the earth's radiation balance. *Rev. Geophys.,* **24,** 422–438.

Cheruy, F., R. S. Kandel, and J. P. Duvel, 1991: Outgoing longwave radiation and its diurnal variations from combined Earth Radiation Budget Experiment and Meteosat observations, 2, Using Meteosat data to determine the longwave diurnal cycle. *J. Geophys. Res.,* **96,** 22 623–22 630.

Doelling, D. R., D. F. Young, R. F. Arduini, P. Minnis, E. F. Harrison, and J. T. Suttles, 1990: On the role of satellite-measured narrowband radiances for computing the earth's radiation balance. Preprints, *Seventh Conf. on Atmospheric Radiation,* San Francisco, CA, Amer. Meteor. Soc., 155–160.

Gruber, A., and J. S. Winston, 1978: Earth–atmosphere radiative heating based on NOAA scanning radiometer measurements. *Bull. Amer. Meteor. Soc.,* **59,** 1570–1573.

——, R. Ellingson, P. Ardanuy, M. Weiss, S.-K. Yang, and S. N. Oh, 1994: A comparison of ERBE and AVHRR longwave flux estimates. *Bull. Amer. Meteor. Soc.,* **75,** 2115–2130.

Harrison, E. F., P. Minnis, and G. G. Gibson, 1983: Orbital and cloud cover sampling analyses for multisatellite earth radiation budget experiments. *J. Spacecraft Rockets,* **20,** 491–495.

——, and Coauthors, 1988: First estimates of the diurnal variation of longwave radiation from the multiple-satellite Earth Radiation Budget Experiment (ERBE). *Bull. Amer. Meteor. Soc.,* **69,** 1144–1151.

——, P. Minnis, B. R. Barkstrom, B. A. Wielicki, G. G. Gibson, F. M. Denn, and D. F. Young, 1990: Seasonal variation of the diurnal cycles of earth's radiation budget determined from ERBE. Preprints, *Seventh Conf. on Atmospheric Radiation,* San Francisco, CA, Amer. Meteor. Soc., 87–91.

Hartmann, D. L., K. J. Kowalewsky, and M. L. Michelsen, 1991: Diurnal variations of outgoing longwave radiation and albedo from ERBE scanner data. *J. Climate,* **4,** 598–617.

Jacobowitz, H., W. L. Smith, H. B. Howell, and F. W. Nagle, 1979: The first 18 months of planetary radiation budget measurements from the *Nimbus-6* ERB experiment. *J. Atmos. Sci.,* **36,** 501–507.

Minnis, P., and E. F. Harrison, 1984: Diurnal variability of regional cloud and clear-sky radiative parameters derived from GOES data. Part I: Analysis method. *J. Climate Appl. Meteor.,* **23,** 993–1011.

——, ——, and G. G. Gibson, 1987: Cloud cover over the eastern equatorial Pacific derived from July 1983 ISCCP data using a hybrid bispectral threshold method. *J. Geophys. Res.,* **92,** 4051–4073.

——, D. F. Young, and E. F. Harrison, 1991: Examination of the relationship between outgoing infrared window and total longwave fluxes using satellite data. *J. Climate,* **4,** 1114–1133.

Raschke, E., and W. R. Bandeen, 1970: The radiation balance of the planet earth from radiation measurements of the satellite *Nimbus-II. J. Climate Appl. Meteor.,* **9,** 215–238.

——, T. H. Vonder Haar, M. Pasternak, and W. R. Bandeen, 1973: The radiation balance of the earth–atmosphere system from *Nimbus-3* radiation measurements. NASA Tech. Note D-7249, 73 pp.

Suttles, J. T., and Coauthors, 1988: Angular radiation models for Earth–atmosphere system; Vol. I, Shortwave radiation. NASA RP-1184, 144 pp.

Taylor, V. R., and L. L. Stowe, 1984: Reflectance characteristics of uniform earth and cloud surfaces derived from *Nimbus-7* ERB. *J. Geophys. Res.,* **89,** 4987–4996.

Wielicki, B. A., and R. N. Green, 1989: Cloud identification for ERBE radiative flux retrieval. *J. Appl. Meteor.,* **28,** 1133–1146.

——, B. R. Barkstrom, E. F. Harrison, R. B. Lee, III, G. L. Smith, and J. E. Cooper, 1996: Clouds and the Earth's Radiant Energy System (CERES): An earth observing system experiment. *Bull. Amer. Meteor. Soc.,* **77,** 853–868.